Journal of
Computational and Theoretical Nanoscience
Vol. 7, 269–276, 2010

Nanoparticle's Size Effect on Its Translocation Across a Lipid Bilayer: A Molecular Dynamics Simulation

Xubo Lin[1, 2], Yang Li[1], and Ning Gu[1, *]

[1] State Key Laboratory of Bioelectronics and Jiangsu Laboratory for Biomaterials and Devices, Southeast University, Nanjing, 210096, P. R. China
[2] Department of Physics, Southeast University, Nanjing, 210096, P. R. China

Understanding the interaction between nanoparticles (NPs) and cell membranes (dipalmitoylphosphatidylcholine or DPPC bilayers) is important for the design of drug delivery systems and provides insights into nanotoxicity. Here we have performed coarse-grained molecular dynamics simulations aimed at nanoparticle's size effect on its translocation across a lipid bilayer. Three hydrophobic nanoparticles of different sizes ranging from 1.284 nm to 2.912 nm are modeled in the simulations. The interaction of NPs induces the structural variations of membranes; the larger the NPs are, the more space they need to cross the bilayer, and the more significant changes the bilayer shows. Some thermodynamics quantities such as free energy have been obtained, indicating that the free energy deceases with the increasing size of NPs. However, no obvious energy barrier can be seen in the free energy profiles during the process of NPs' transport. The translocation time of NPs to different positions of the bilayer has also been calculated based on the free energy. The results show that the size of NPs affects the translocation time differently. Our simulation results suggest that the size of NP has significant impacts on its translocation across the lipid bilayer.

Keywords: Size, Nanoparticle, Molecular Dynamics, Lipid Bilayer.

1. INTRODUCTION

The extent of the production and use of nanopartices (NPs) is rapidly growing, largely increasing the possibility of exposures to various NPs. However the biological influences of NPs depend on their various unique features, such as size, hydrophobicity, chemical composition, shape, surface charge density, and aggregation.[1] These features can affect cellular uptake, binding and activation of membrane receptors, protein binding and translocation to the target tissues.[2, 3] Hence, obtaining more information about the interactions between NPs and biological systems, especially cell membrane, will be of great use to develop potential applications and to avoid possible toxicity.

Size is an important factor in the interaction between NPs and cell membrane. It can affect NPs' nonspecific uptake in cells, with potential to induce cellular responses.[4–6] For manipulation or detection of biological structures and systems, modifying the size effect of nanoparticles can facilitate the performance of NPs in imaging,[7] biosensing[8] and gene and drug delivery.[9] From the perspective of NP-membrane interaction, many recent researches, demonstrating different response mechanisms of the lipid bilayer induced by the size of NPs, have been reported in experiments[10–12] and in computer simulations.[13, 14] Gao et al.[15] have reported that the quantity of NP-delivered drugs across blood brain barrier is size-dependent. As Jiang et al.[4] have reported, the binding and activation of membrane receptors and subsequent protein expression strongly depend on nanoparticles' size. Besides, these microcosmic processes of interactions between carbon NPs and membrane have received recent attention.[4, 12, 16] But the size effect of NPs on their translocations across a membrane at a molecular level has not been studied systematically.

In the present paper we investigated the size effect of hydrophobic nanoparticles on their translocations across a lipid bilayer by molecular dynamics simulations. Some simulation details are given in Section 2. In Section 3, we provide some statistical analysis of simulations.

*Author to whom correspondence should be addressed.

2. SIMULATION DETAILS

All simulations in this paper were performed with the MARTINI force field developed by Marrink et al.[17-18] In this force field, a coarse-grained (CG) model to reproduce experimental properties of various lipid assemblies was defined. The CG model includes four main types of interaction sites: polar (P), nonpolar (N), apolar (C), and charged (Q). For particles of type N and Q four subtypes (d = donor, a = acceptor, da = both, 0 = none) are further distinguished to denoting the hydrogen-bonding capabilities; for particles of type P and C, subtypes are distinguished by a number indicating the degree of polarity (from 1, low polarity, to 5, high polarity). A CG DPPC molecule is comprised of 12 beads. The headgroup (head) includes two charged beads: one bead (Q0) for the choline (NC3) with one unit of positive charge and one bead (Qa) for the phosphate (PO_4) with one unit of negative charge. Two nonpolar beads (Na) compose the glycerol ester backbone (GLY). Each of two tails (tail) consists of four apolar beads (C1), of which each methylene unit is mapped into a tail bead. For a CG water (W), each bead (P4) represents four water molecules.

We constructed three NPs of different sizes (diameter: NP1 $\sim$ 1.284 nm, NP2 $\sim$ 2.098 nm, NP3 $\sim$ 2.912 nm) according to the simple-cubic-lattice structure. NP1 consists of 8 beads; NP2, 27 beads; NP3, 64 beads. All beads used for NPs are the same type (C1) as DPPC tail to represent their hydrophobic property. To restrict bonds and bond angles, the force constants applied to NPs are as same as that used for DPPC molecules. In addition, diagonal bond restricts in simple cubic lattice are also considered. In other words, the NPs are more "rigid" than DPPC molecules, except they are allowed to deform in a certain degree.

An initial configuration file was downloaded from http://md.chem.rug.nl/~marrink/coarsegrain.html. The system includes 128 DPPC molecules and 2000 water molecules with the box dimensions of $6.32 \times 6.46 \times 10.05$ nm^3. Then we enlarged the system size to 512 DPPC molecules and 18020 water molecules with box dimensions of $12.98 \times 13.58 \times 16.24$ nm^3. After energy minimization, an equilibration of 40 ns were performed with a time step of 40 fs. The final equilibrium configuration was used as the starting state for the next simulations.

All simulations were performed with GROMACS 3.3.3 simulation package.[19] The Berendsen thermostat and barostat[20] were used to maintain a constant temperature of 325 K and a constant pressure of 1 bar in the NPT ensemble. A cutoff of 1.2 nm was used for van der Waals interactions. With use of the standard shift function of GROMACS in which both the energy and force vanish at the cutoff distance, the Lennard-Jones (LJ) potential was smoothly shifted to zero between 0.9 and 1.2 nm to reduce the cutoff noise. For electrostatic interactions, the Coulombic potential, with a cutoff of 1.2 nm, was also smoothly shifted to zero from 0 to 1.2 nm.[17,18]

To facilitate the following discuss, we define mid-plane of DPPC bilayer as X–Y plane, with Z axis perpendicular to the bilayer. At first, the system is copied into three same systems. Then, we put NP1, NP2, NP3 into these systems separately to obtain three new systems, each with single NP. After energy minimization, the nanoparticle is position-restrainted with a force constant of 8000 kJ mol^{-1} nm^{-2}, and a pre-equilibration run of 10 ns has been performed in order to remove incorrect overlaps and obtain a stable configuration. This configuration represents the state that NP is close up to membrane, but doesn't induce significant changes. Then three 40 ns separate molecular dynamics (MD) simulations have been performed with the obtained stable configurations. Besides, constraint mean force (CMF) simulations[21] have been performed in order to compute the free energy profile of NP separately.

3. RESULTS AND DISCUSSION

After 40 ns equilibration run, we analyze the simulation trajectory for getting the density profile of DPPC bilayer, shown in appendix A. The thickness of lipid bilayer is about 4.18 nm. The average area per lipid (Aav) is 0.648 nm^2, computed using the method given in Ref. [22].

3.1. Structural Changes During the Translocation

The boundary of the bilayer in the z-direction is defined by peak density of headgroup. Figures 1(a), (b) and (c) show the evolutions of the z-position of NP1, NP2 and NP3. Inset A shows the histogram of the z-coordinate of the center-of-mass of NP after $t = 3$ ns (at that time, NP entered the bilayer completely). Inset B shows the final configuration of system in the simulation. The initial positions of NP1, NP2 and NP3 were $z = 2.287$ nm, $z = 2.663$ nm and $z = 2.919$ nm. Soon after $t = 1.72$ ns, $t = 0.52$ ns and $t = 0.76$ ns, NP1, NP2 and NP3 "jumped" into the bilayer. And we observe the most probable z-positions of NP1, NP2 and NP3 are $z \approx -0.02$ nm, $z \approx -0.05$ nm and $z \approx 0.0$ nm. Besides, all NPs adsorbed deeply in the bilayer were wrapped by the lipid tails tightly.

In our simulations, NPs were placed near the surface of the bilayer. All NPs "jumped" into the bilayer easily and preferred the location around the mid-plane of bilayer ($z = 0$).

The penetration of small hydrophobic NPs into the lipid bilayer is usually hypothesized to be induced by the formation of pores in the lipid membrane.[16] Voronoi analysis were given in Figure 2 to describe a intuitionistic picture of the topology structure fluctuation in the bilayer just before NP entered the bilayer. We observe that space

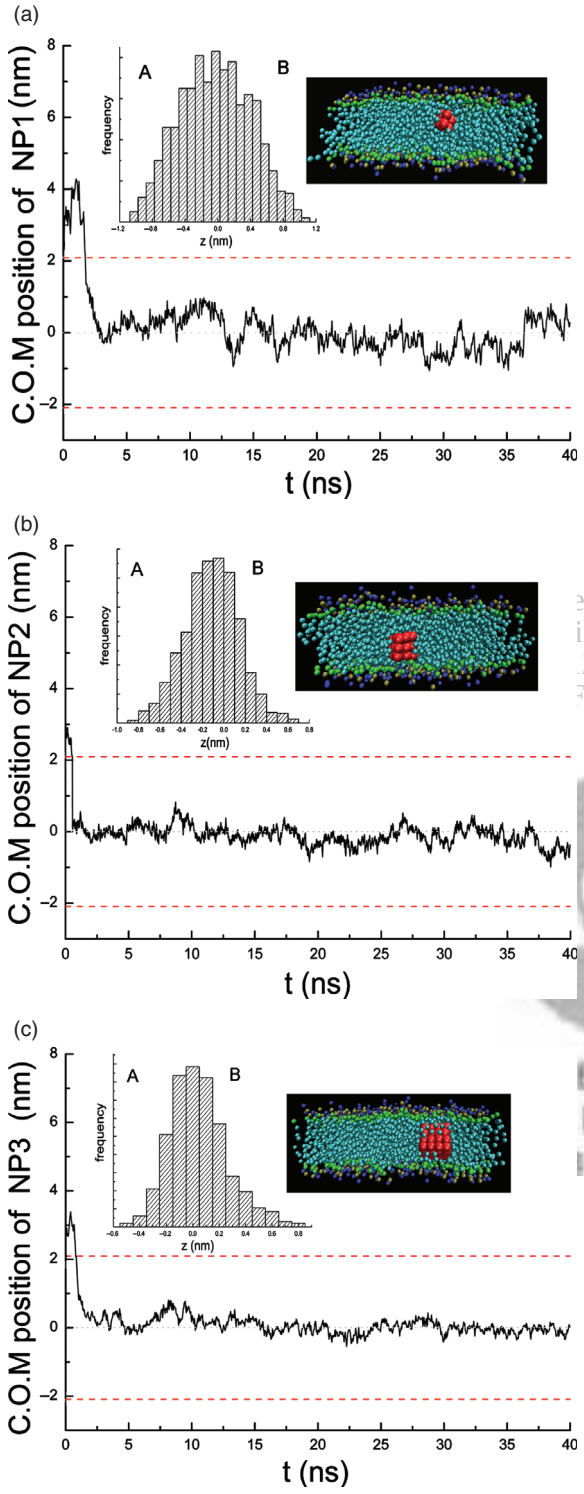

Fig. 1. Trajectories of NPs in the transmembrane (z) direction. The two dashed line represent locations of headgroup peak density of the upper and lower leaflet of DPPC bilayer. Panel (a) is for NP1, Panel (b) for NP2, Panel (c) for NP3. (A) The histogram of the z-coordinate of the center-of-mass of NP after NP enters the bilayer ($t > 3$ ns); (B) the side view of the simulation system at $t =$ 40 ns. The red beads denote NP, cyan beads denote the lipid tail groups, green beads denote GLY, and the tan and blue beads represent the lipid head groups. The explicit water molecules as well as DPPC molecules before NP are omitted for clarity. The snapshots were rendered using VMD.[23]

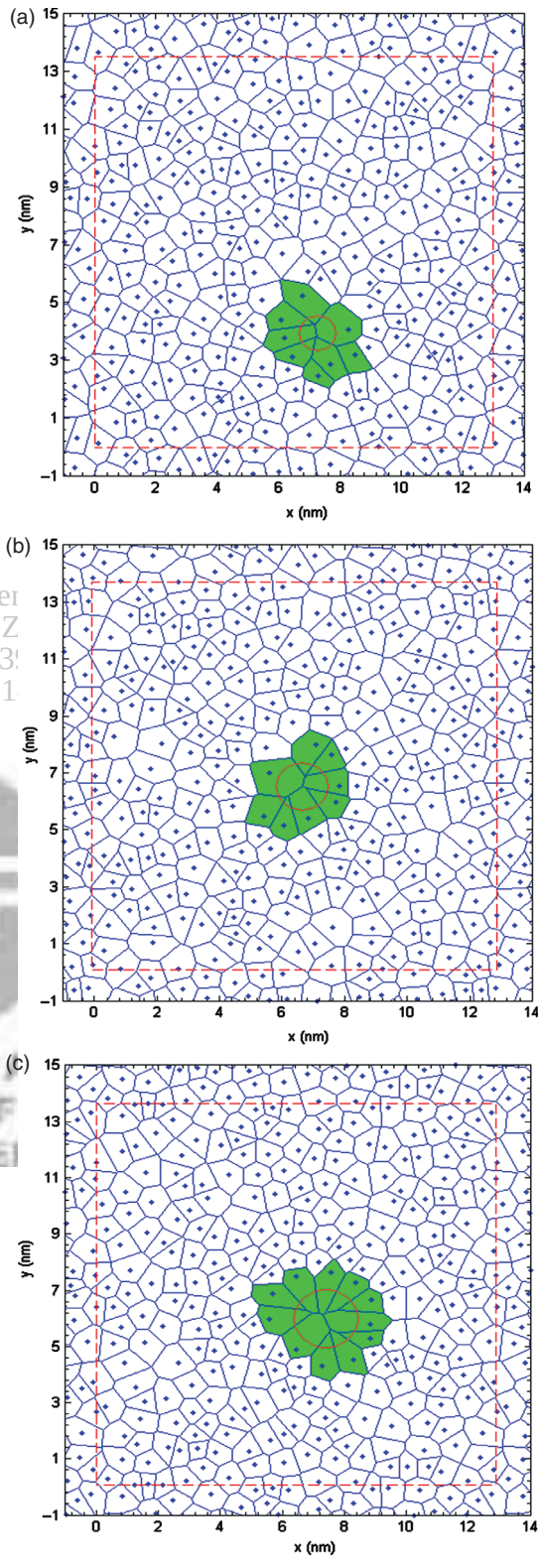

Fig. 2. Voronoi tessellations of the top leaflet of DPPC bilayer at the time just before the NP "jumped" into the lipid bilayer. (a) is for NP1, (b) for NP2, (c) for NP3. Each cell represents a lipid head. The dots denote the center-of-mass of the DPPC head groups and the circle denotes the position of NP on the xy-plane. The shaded cells correspond to the lipid head groups that are adjacent to the NP. The dashed lines represent the periodic boundary.

among lipid head groups adjacent to all three NPs is large, therefore pore has formed. The average area of shaded regions adjacent to NP1 is 1.001 nm^2, 54.5% larger than Aav. The average area of shaded regions adjacent to NP2 is 1.062 nm^2, 63.9% larger than Aav. The average area of shaded regions adjacent to NP3 is 1.083 nm^2, 67.1% larger than Aav. Larger NP needs more space to cross the bilayer, therefore forms larger pore.

After NP penetrating into lipid bilayer, it will induce some structural changes. To understand these structural changes of bilayer, we calculate the average area per lipid head[22] as a function of the lateral distance between the lipid head group and NP, shown in Figure 3. Two periods of time representing NP with different distances from the mid-plane of DPPC bilayer were studied (shown in insets A and B, with B representing farther distance). For NP1, average area per lipid head at all lateral distances shows no significant difference (<4%) in both two periods. This indicates that after NP1 entered the bilayer, no obvious local configuration changes occurred. For NP2, in the time period I ($t = 8$ ns–$t = 8.6$ ns), average area per lipid head within the range of ~0.5 nm exceeds Aav a lot(maximum~12.65%). Besides, region of $z = 0.7$ nm–$z = 2$ nm appears tight lipid arrangement with average area per lipid head lower than Aav(maximum~7.4%). In the time period II ($t = 8.6$ ns–$t = 8.98$ ns), average area per lipid head within the range of ~1.4 nm exceeds Aav a lot(maximum~12.75%). For both two time periods, region of $z > 2$ nm isn't affected too much. This indicates that when NP2 located in the bilayer interior, its movement induced relatively large local configuration changes which formed pore. Besides, the size of the pore increases with the distance between NP2 and mid-plane of DPPC bilayer. Although pore formed, no water molecules were found to enter the pore in our simulation. For NP3, in the first time period I ($t = 6.12$ ns–$t = 7.6$ ns), average area per lipid head within the range of ~0.7 nm exceeds Aav a lot(maximum~23.5%). In the time period II ($t = 7.6$ ns–$t = 8.36$ ns), average area per lipid head within the range of ~0.7 nm exceeds Aav a lot(maximum ~38.0%). For both two time periods, region of $z > 0.7$ nm is affected more than NP1, NP2. This indicates that after NP3 remained in the bilayer, its movement will induce relatively large local configuration changes which form pore. Besides, the size of the pore increase with the distance between NP3 and mid-plane of DPPC bilayer, and the range of NP3's effect is larger. Although pore formed, still no water molecules were found to enter the pore in our simulation.

When NP is about to "jump" into the DPPC bilayer, the average area adjacent to NP increases with size of NP. In all three situations, an obvious pore formed. After NP entered the DPPC bilayer, the smaller size it has, the less influence on the fluctuation of the DPPC bilayer. As NP's size increase, the area of induced pore and the range

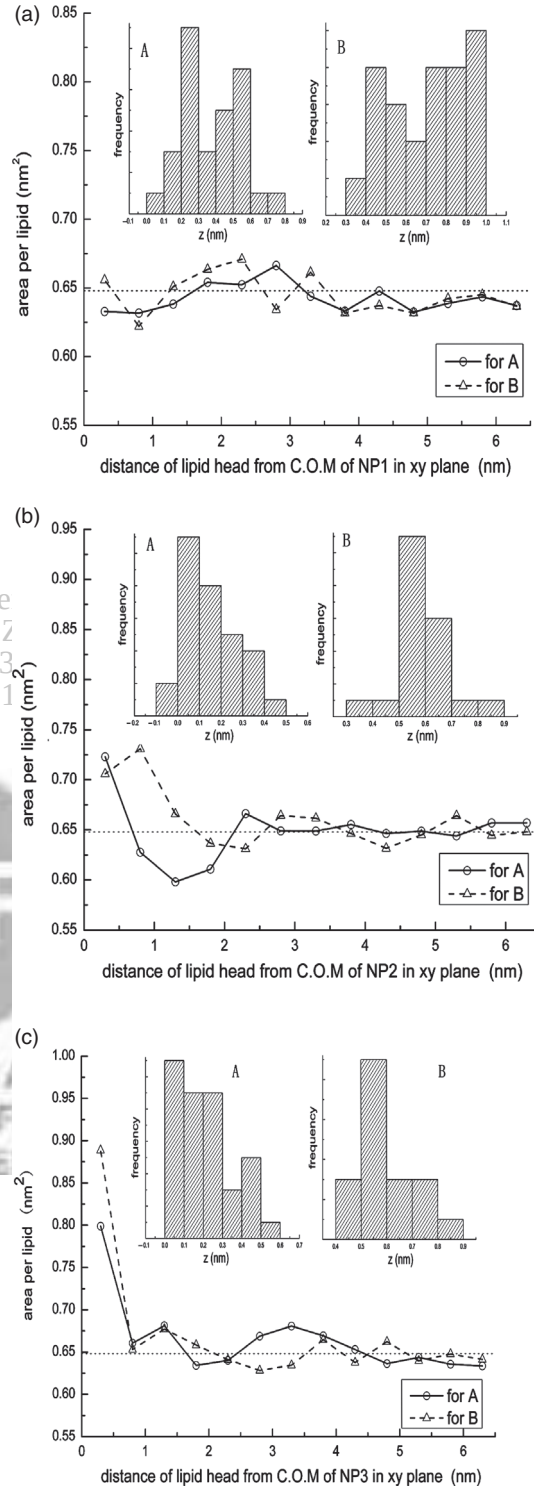

Fig. 3. Average area per lipid head as a function of the lateral distance between the lipid head group and NP adsorbed into the lipid bilayer. For each NP, two time periods (labeled as I and II) have been studied. (a) The solid line is for time period I, and the dashed line is for time period II. The thin dotted line denotes the average head area of lipid (Aav = 0.648 nm^2). The histograms of the z-coordinate of NP during these two periods are shown in insets A and B, respectively. (a) is for NP1: I ($t = 9$ ns–$t = 10.2$ ns), II ($t = 10.2$ ns–$t = 11.08$ ns); (b) is for NP2: I ($t = 8$ ns–$t = 8.6$ ns), II ($t = 8.6$ ns–$t = 8.98$ ns); (c) is for NP3: I ($t = 6.12$ ns–$t = 7.6$ ns), II ($t = 7.6$ ns–$t = 8.36$ ns).

it affects become larger. In addition, the area of induced "micropore" varies with the distance between NP and mid-plane of DPPC bilayer. No water molecules were found to transport through the pore in our simulation. Whether the varied "micropore" has correlations with the deposit of small hydrophobic NPs in the tissues such as lung[24] still needs to be researched more.

3.2. Calculate the Mean Time of NP Translocating into the Bilayer

The process that NP translocate into bilayer can be described by (on the assumption that correlation time of Γ is very small):[25]

$$m\ddot{z}(t)+\gamma(z)\dot{z}(\tau)+\frac{dG(z)}{dz}=\Gamma(z,t) \quad (1)$$

$$\langle\Gamma(z,t)\Gamma(z,t+\tau)\rangle=2k_{\mathrm{B}}T\gamma(z)\delta(\tau) \quad (2)$$

$$\langle\Gamma(z,t)\rangle=0 \quad (3)$$

Here $\langle\ldots\rangle$ means an average over the simulation, m is the mass of the nanoparticle, γ is the time-independent friction coefficient, G is the free energy, and Γ is the normally distributed random force with zero mean, k_B is the Boltzmann constant, T is the system temperature, δ is the Dirac delta function.

When using Constraint Mean Force (CMF) method,[21, 28] the force acting on the center of mass of the solute at a chosen z depth is obtained at each time step as the negative of the force required to maintain the z-constraint and is indicated as $F(z,t)$. So Eq. (1) can be changed into:

$$\frac{dG(z)}{dz}=\Gamma(z,t)+F(z,t) \quad (4)$$

Combine (3)(4), we get

$$G(z)-G(z=4.7\text{ nm})=-\int_{z=4.7\text{ nm}}^{z}\langle F(z,t)\rangle dz \quad (5)$$

Here we simply define $G(z=4.7\text{ nm})=0$ kJ/mol Diffusion coefficient $D(z)$ can be obtained[21, 25] by (2):

$$D(z)=\frac{(k_{\mathrm{B}}T)^2}{\int_0^\infty\langle\Gamma(z,t)\Gamma(z,t+\tau)\rangle d\tau} \quad (6)$$

Then, the mean time $\langle\tau_{\mathrm{trn}}(z_1\rightarrow z_2)\rangle$ for NP[21, 25] moving across the bilayer from z_1 to z_2 is:

$$\langle\tau_{\mathrm{trn}}(z_1\rightarrow z_2)\rangle=\frac{1}{D}\int_{z_1}^{z_2}e^{G(y)/k_{\mathrm{B}}T}\,dy\int_{z_1}^{y}e^{-G(x)/k_{\mathrm{B}}T}\,dx \quad (7)$$

where D is the average diffusion coefficient.

The adsorption of hydrophobic NP into the lipid bilayer is driven by the hydrophobic interactions between NP and the lipid tails. As the size of NP increases, the hydrophobic interactions become stronger. But meanwhile, difficulty to pile out lipid molecules vacating more space goes up. To get a more quantitative picture, we performed additional simulations to calculate the free energy of NP using CMF method.[21] This method requires the center of mass of the permeant particle to be constrained at chosen depths in the membrane. In our simulations, we choose 48 different positions from $z=0$ nm to $z=4.7$ nm (step = 0.1 nm) for each NP. For each of these simulations, a pre-equilibrium run of 1 ns was first performed so that the system reached equilibrium, and this was followed by a simulation of 10 ns during which the average force was calculated. Results from one leaflet were considered valid for the other layer too, for reasons of symmetry.

Figure 4 is the free energy profile obtained by using Eq. (5). There are no energy barriers for all NPs considered in our paper. This is consistent with large NP's free energy in Ref. [26]. Larger NP has dramatic downtrend for its free energy profile. This implies that the hydrophobic interactions between NP and the lipid tails play a dominant role and all NPs tend to translocate to mid-plane of the DPPC bilayer. This is supported by the above simulations in our paper. As for NP1, when far from the bilayer, the hydrophobic interactions between NP1 and the lipid tails is so weak that the free energy profile is rather flat.

To validate the statistical analysis used in our paper, we calculated the random force fluctuation autocorrelation functions for three NPs to estimate the correlation time of random force Γ. Only four different positions (chosen according to Four Region Model in Ref. [27]) are shown for each NP in the Appendix B. By analyzing all autocorrelation functions curves shown and unshown, we find correlation time of Γ is less than 1 ps. This implies the assumption used for Eqs. (1) and (2) is reasonable.

Then we calculated the diffusion coefficient of NP at different positions, and the obtained diffusion coefficient

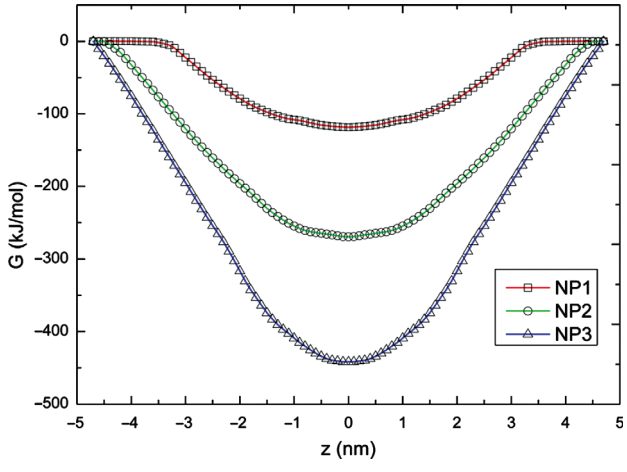

Fig. 4. Free energy profile. The red line is for NP1, the green line for NP2 and the blue line for NP3. *Note*: 1 kcal = 4.184 kJ.

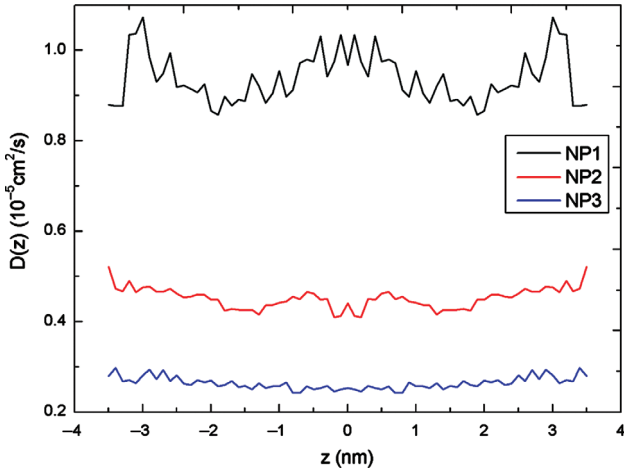

Fig. 5. Diffusion coefficient profiles of three NPs near and inside the DPPC bilayer. Black line is for NP1, red line for NP2, blue line for NP3.

profile is as Figure 5. Due to potential deviation from reality while using MARTINI[17, 18] force field, only the average diffusion coefficient was considered. We observed the average diffusion coefficient decreases with the size of NP.

Figure 6 shows mean time needed for NPs permeating to different positions near and inside the DPPC bilayer using Eq. (7). We observe that time needed for NP permeating to positions of $z > 0.35$ nm decreases with the size of NP. As previous simulations shows, the larger the NP is, the more difficult it is to pile out lipid molecules vacating more space for translocation. In another word, the trend of these changes implies that the hydrophobic interactions between NPs and the lipid tails increase more rapidly than the difficulty to go across the bilayer. We also observe that when NP is very near to the mid-plane of the DPPC bilayer, the trend of changes seems irregular.

The accuracy of the simulations was affected by proper sampling of $F(z, t)$, so we monitor this accuracy by looking at the convergence of the value of $\langle F(z, t)\rangle$ within different simulation times. Only three different positions ($z = 0$ nm, 1.60 nm, 3.00 nm for mid-plane, peak density and bulk water position) for each NP are shown in Appendix C. We observed $\langle F(z, t)\rangle$ at both shown and unshowed positions converges to a certain value within 4 ns. To avoid improper sampling, 10 ns simulation for calculate $F(z, t)$ was performed for each position. From this perspective, the sampling in our simulations is proper, and the subsequent calculations is reasonable.

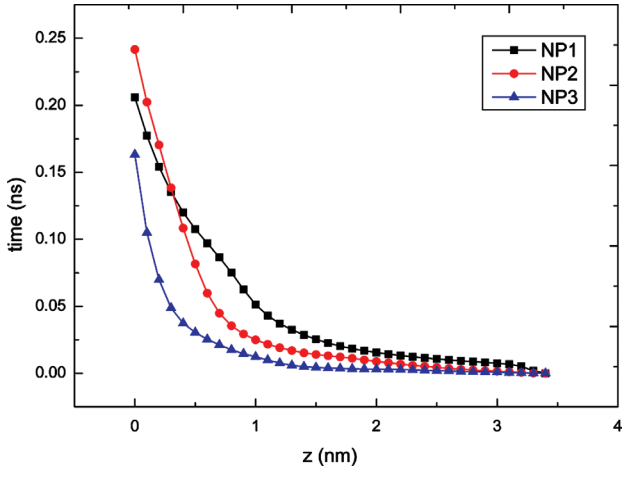

Fig. 6. Time needed for NPs permeating to different positions ($z = 3.4$–0 nm) near and inside the DPPC bilayer. Black line is for NP1, red line for NP2, blue line for NP3.

4. CONCLUSION

With coarse-grained molecular dynamics simulations, we investigated NP's size effect on translocation across the DPPC bilayer. Three NPs of different sizes were considered in our simulations. When NP is about to "jump" into the DPPC bilayer, the average area adjacent to NP increases with size of NP. After NP permeates into the DPPC bilayer, the larger NP's size, the wider the area of induced pore and the range it affects. In addition, the area of induced pore varies with the distance between NP and mid-plane of DPPC bilayer. As for free energy profiles, larger NP has dramatic downtrend, all showing no significant energy barrier before they "jump" into the bilayer interior. And the time needed for translocation to different positions in bilayer (except for regions very near the mid-plane of the DPPC bilayer) decreases with the size of NPs.

APPENDIX

A. Density Profile

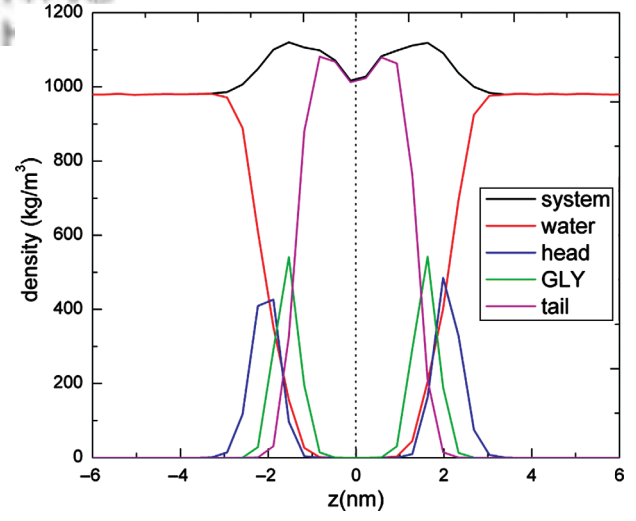

Fig. A1. Density profile of DPPC bilayer along z axis. The black line represents the system density, the red line for water molecules, the blue line for headgroup of DPPC molecules, the green line for GLY of DPPC molecules and the magenta line for tail group of DPPC molecules.

B. Random Force Fluctation Autocorrelation Functions

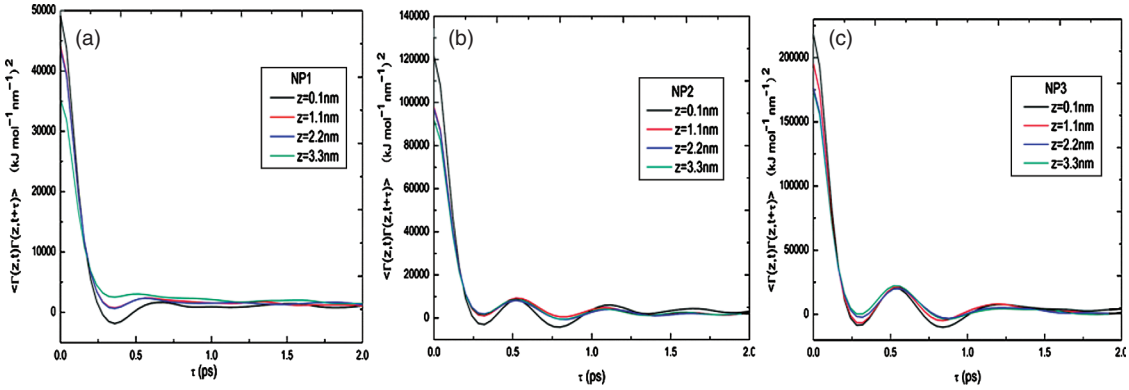

Fig. B1. Random force fluctuation autocorrelation functions. (a) for NP1; (b) for NP2; (c) for NP3. Only four different positions (chosen according to Four Region Model in Ref. [14]) are shown in this figure.

C. Data Convergence

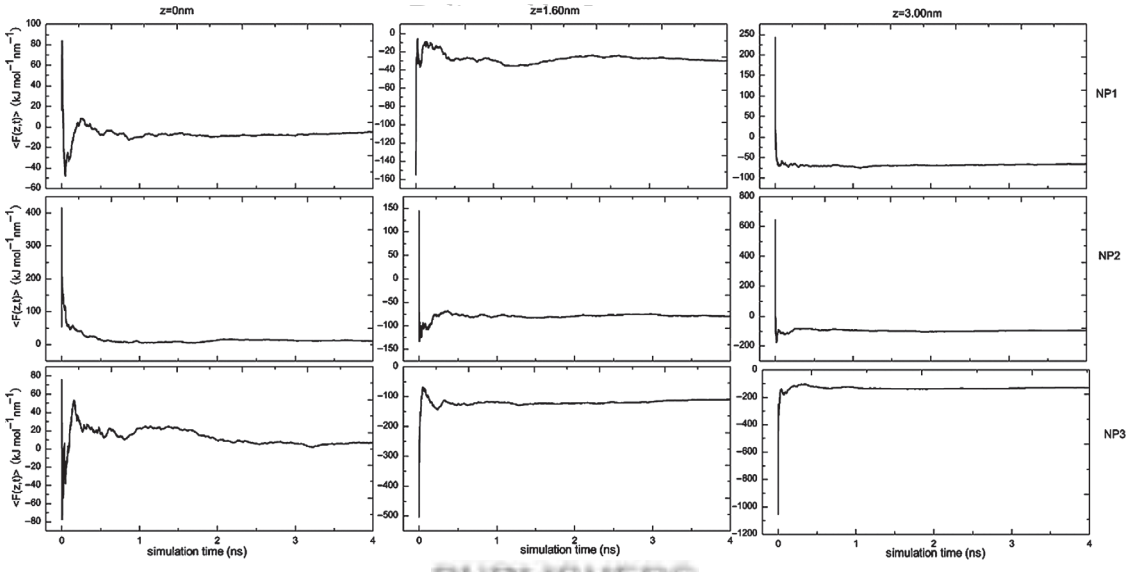

Fig. C1. Values of $\langle F(z,t)\rangle$ as a function of the simulation time. Only three different positions(z) are shown for NPs each for clarity.

Acknowledgments: We gratefully acknowledge the support to this research from the National Natural Science Foundation of China for financial support of this research (Grants 50872021) and the National Important Basic Research Program of China (Grants 2006CB933206 and 2006CB705606).

References

1. A. Nel, T. Xia, L. Madler, and N. Li, *Science* 311, 622 (**2006**).
2. G. Oberdorster, E. Oberdorster, and J. Oberdorster, *Environ. Health Perspect.* 113, 823 (**2005**).
3. M. P. Desai, V. Labhasetwar, G. L. Amidon, and R. J. Levy, *Pharm. Res.* 13, 1838 (**1996**).
4. W. Jiang, B. S. Kim, J. T. Rutka, and C. W. Chan, *Nat. Nanotechnol.* 3, 145 (**2008**).
5. B. D. Chithrani, A. A. Ghazani, and W. C. W. Chan, *Nano Lett.* 6, 662 (**2006**).
6. S. Shortkroff, M. Turell, K. Rice, and T. S. Thornhill, *Mater. Res. Soc. Symp. Proc.* 704, W11.5.1 (**2002**).
7. I. H. El-Sayed, X. Huang, and M. A. El-Sayed, *Nano Lett.* 5, 829 (**2005**).
8. I. Medintz, A. R. Clapp, J. S. Melinger, J. R. Deschamps, and H. Mattoussi, *Adv. Mater.* 17, 2450 (**2005**).
9. N. Kohler, C. Sun, J. Wang, and M. Zhang, *Langmuir* 21, 8858 (**2005**).
10. Y. Roiter, M. Ornatska, A. R. Rammohan, J. Balakrishnan, D. R. Heine, and S. Minko, *Nano Lett.* 8, 941 (**2008**).
11. B. D. Chithrani, A. A. Ghazani, and W. C. W. Chan, *Nano Lett.* 6, 662 (**2006**).
12. F. Osaki, T. Kanamori, S. Sando, T. Sera, and Y. Aoyama, *J. Am. Chem. Soc.* 126, 6520 (**2004**).
13. V. V. Ginzburg and S. Balijepalli, *Nano Lett.* 7, 3716 (**2007**).
14. A. Chang and A. Violi, *J. Phys. Chem. B* 110, 5073 (**2006**).
15. K. Gao and X. Jiang, *Int. J. Pharm.* 310, 213 (**2006**).
16. R. Qiao, A. P. Roberts, A. S. Mount, S. J. Klaine, and P. C. Ke, *Nano Lett.* 7, 614 (**2007**).

17. S. J. Marrink, A. H. de Vries, and A. E. Mark, *J. Phys. Chem. B* 108, 750 **(2004)**.
18. S. J. Marrink, H. J. Risselada, S. Yefimov, D. P. Tieleman, and A. H. de Vries, *J. Phys. Chem. B* 111, 7812 **(2007)**.
19. E. Lindahl, B. Hess, and D. V. der Spoel, *J. Mol. Model.* 7, 306 **(2001)**.
20. H. J. C. Berendsen, J. P. M. Postma, W. F. V. Gunsteren, A. DiNola, and J. R. Haak, *J. Chem. Phys.* 81, 3684 **(1984)**.
21. D. Bemporad, J. W. Essex, and C. Luttmann, *J. Phys. Chem. B* 108, 4875 **(2004)**.
22. W. J. Allen, J. A. Lemkul, and D. R. Bevan, *J. Comput. Chem.* 30, 1952 **(2009)**.
23. W. Humphrey, A. Dalke, and K. Schulten, *J. Mol. Graphics* 14, 33 **(1996)**.
24. G. Oberdorster, J. Ferin, and B. E. Lehnert, *Environ. Health Perspect.* 102, 173 **(1994)**.
25. C. W. Gardiner, Handbook of Stochastic Methods for Physics, Chemistry and the Natural Sciences, 2nd edn., Springer-Verlag, Berlin, Heidelberg, New York **(1985)**.
26. Y. Li, X. Chen, and N. Gu, *J. Phys. Chem. B* 112, 16647 **(2008)**.
27. S. J. Marrink and H. J. C. Berendsen, *J. Phys. Chem.* 100, 16729 **(1996)**.
28. R. A. Tasseff and D. I. Kopelevich, *J. Undergraduate Research* 7 **(2006)**.

Received: 2 June 2009. Accepted: 16 June 2009.